sustainability

MDPI

Article

Confinement Effect of Reinforced Concrete Columns with Rectangular and Octagon-Shaped Spirals

Hyeong-Gook Kim, Chan-Yu Jeong, Dong-Hwan Kim and Kil-Hee Kim *

Department of Architectural Engineering, Kongju National University, Cheonandaero, Seobuk, Cheonan 1223-24, Korea; anthk1333@kongju.ac.kr (H.-G.K.); ssbachany@kongju.ac.kr (C.-Y.J.); kimdh@kongju.ac.kr (D.-H.K.)

* Correspondence: kimkh@kongju.ac.kr; Tel.: +82-41-521-9335

Received: 29 August 2020; Accepted: 24 September 2020; Published: 26 September 2020

Abstract: Conventional spiral-type transverse reinforcement is effective at increasing the ductility and the maximum strength of reinforced concrete (RC) columns because it confines the inner concrete and the longitudinal reinforcement. However, when arranging crossties in a RC column with spirals, problems such as mutual interference with longitudinal reinforcement, overcrowding of reinforcement, and deterioration of constructability occur. Furthermore, the loosening of 90 and 130-degree standard hooks due to the lateral expansion of concrete causes buckling of the longitudinal reinforcement. This paper describes the ability of a newly developed spiral-type transverse reinforcement with various yield strengths to confine RC columns subjected to cyclic lateral load and constant axial load. The ductility capacity, energy dissipation, and effective stiffness of RC columns confined by the developed spiral-type transverse reinforcement were compared with those of RC columns confined by typical rectangular reinforcement. The experimental results showed that RC column specimens with the developed spiral-type transverse reinforcement have better performances in terms of ductility capacity and energy dissipation, even though the amount of reinforcement used for the specimens decreased by about 27% compared with the specimen with typical rectangular reinforcement.

Keywords: reinforced concrete column; confinement effects; energy dissipation

1. Introduction

Reinforced concrete (RC) columns subject to both central axial load and flexural load undergo a rapid deterioration of strength due to lateral expansion of inner concrete after delamination of the concrete cover. At this point, transverse reinforcement of RC columns confines the lateral expansion of core concrete, thus increasing the compressive strength and ductility under lateral load. The lateral confinement performance of RC columns is influenced by the strength ratio of transverse reinforcement and concrete, the amount and shape of transverse reinforcement, and the shear span to depth ratio [1–10]. Many models have been developed based on experiments to predict the strength and behavior of RC columns and concrete cylinders with shear reinforcement [11–18]. Extensive research has also been conducted not only on conventional crossties, but also on interlocking spirals to suppress lateral expansion of core concrete and buckling of longitudinal reinforcement, as well as shear reinforcement of RC columns using Fiber-Reinforced Polymer (FRP) [19–27].

Transverse reinforcement of RC columns can be largely classified into crossties and spiral reinforcement. Compared to crossties, spiral reinforcement can effectively confine the inner concrete of RC columns, and is thus more advantageous in enhancing ductility. However, due to difficulties in bar arrangement during construction, there is a higher demand for columns with rectangular cross-sections than for those with circular cross-sections. As such, most columns have shear reinforcement in the form of crossties, which are also more common than spiral reinforcement even in rarer columns with

circular cross-sections. In terms of ductility enhancement, introducing sub-ties is more efficient than decreasing the spacing of transverse reinforcement. Sub-ties are effective at suppressing the lateral expansion of core concrete, and also prevent the buckling of longitudinal reinforcement. The use of conventional sub-ties with 90-degree and 135-degree standard hooks can result in problems such as mutual interference with longitudinal reinforcement, overcrowding of reinforcement, poor filling of concrete, and deterioration of constructability. When subject to repeated lateral forces such as seismic loads, the loosening of 90-degree hooks causes a decrease in effective lateral confinement, which may contribute to buckling and weakening of longitudinal reinforcement.

This study proposed a new type of transverse reinforcement with spirally arranged crossties to improve the constructability of RC columns and to resolve structural issues associated with conventional crossties. Cyclic loading tests were performed on RC columns with the new spiral-type transverse reinforcement and subject to a central axial load. The effects of transverse reinforcement shape and yield strength on crack formation, ductility capacity, energy dissipation capacity, and effective stiffness in relation to drift angle were assessed. In addition, the constructability of RC column members was evaluated by measuring time consumed in arranging the proposed transverse reinforcement.

2. Experimental Program

2.1. Materials

The concrete mixture specifications are given in Table 1. Ready-mixed concrete with a design strength of 24 MPa was used to manufacture the specimens, as described in Table 1. Concrete cylinders with dimensions of ϕ100 mm × 200 mm were manufactured in accordance with ASTM C31/C31M. The compressive strength of the concrete was tested according to ASTM C39/C39M. The mean compressive strength of concrete measured in the cylinder test was 22.4 MPa. This value was used to predict the shear strength of specimens.

Table 1. Proportions of concrete mixture.

f'_c	G_{max}	W/C	S/a	Unit Weight(kg/m^3)					Slump
(MPa)	(mm)	(%)	(%)	W	C	S	G	AD	(mm)
24	25	49.7	48.5	82	214	872	936	69.3	120

f'_c: compressive strength of concrete, G_{max}: maximum size of coarse aggregate, W/B: water binder ratio, S/a: fine aggregate modulus, W: water, C: cement, S: fine aggregate, G: coarse aggregate, and AD: water reducing admixture.

Two types of reinforcing bars were used to manufacture the specimens. D19 (286.7 mm^2) deformed bars with a yield strength of 523 MPa were used for longitudinal reinforcement of all specimens. D10 (71.3 mm^2) deformed bars with yield strengths of 540 MPa, 554 MPa, 788 MPa, and 1328 MPa were used for transverse reinforcement. Table 2 shows the physical properties of the reinforcing bars.

Table 2. Mechanical properties of reinforcing steel.

Specimen	Reinf. Bar	f_y (MPa)	ε_y	E_s (MPa)	Remarks
H-F	D10	540	0.0027	200,000	
KSS-5	Φ10	554	0.0028	197,857	Transverse reinforcement
KSS-7	Φ10	788	0.0039	202,051	
KSS-12	Φ10	1328	0.0066	201,212	
All Specimens	D19	523	0.0028	186,586	Longitudinal reinforcement

f_y: yield strength of reinforcement, ε_y: yield strain of reinforcement, and E_s: modulus of elasticity.

2.2. Specimen Details

To evaluate the lateral confinement effect of RC columns in relation to shape and strength of transverse reinforcement, this study fabricated four specimens as shown in Table 3. H-F refers to RC

column specimens with rectangular transverse reinforcement, while KSS-5, KSS-7, and KSS-12 are specimens with the proposed KSS-transverse reinforcement comprised of rectangular and octagonal spirals. The numbers 5, 7, and 12 in the KSS specimen name represent the yield strength grade of the proposed transverse reinforcement, that is, 500 MPa, 700 MPa, and 1200 MPa, respectively.

Table 3. Properties of specimens.

Specimen	f'_c (MPa)	ρ_w (-)	f_{wy} (MPa)	$\rho_w f_{wy}$ (MPa)	B (mm)	D (mm)	d (mm)	s (mm)	v (mm^3)
H-F	22.4	0.0051	540	2.75	450	450	400	125	235,504
KSS-5		0.0037	554	2.04					171,387
KSS-7			788	2.91					
KSS-12			1328	4.90					

f'_c: compressive strength of concrete, ρ_w: volume ratio of transverse reinforcement, f_{wy}: yield strength of transverse reinforcement, s: spacing of transvere reinforcement, and v: volume of transvere reinforcement.

Figure 1 shows details of bar arrangement of H-F specimens with conventional rectangular transverse reinforcement and KSS specimens with the proposed spiral-type shear reinforcement. As shown in Figure 1, rectangular crossties were spaced 125 mm apart in H-F specimens, and sub-ties having 90-degree and 135-degree bending angles in longitudinal and lateral directions as specified in the ACI design code were arranged with the same spacing. As shown in Figure 1b, KSS specimens had rectangular crossties and octagonal sub-ties arranged spirally to facilitate confinement of longitudinal reinforcement at the edges and inner longitudinal reinforcement. The rectangular crossties were given the same spacing as the crossties of the H-F specimens.

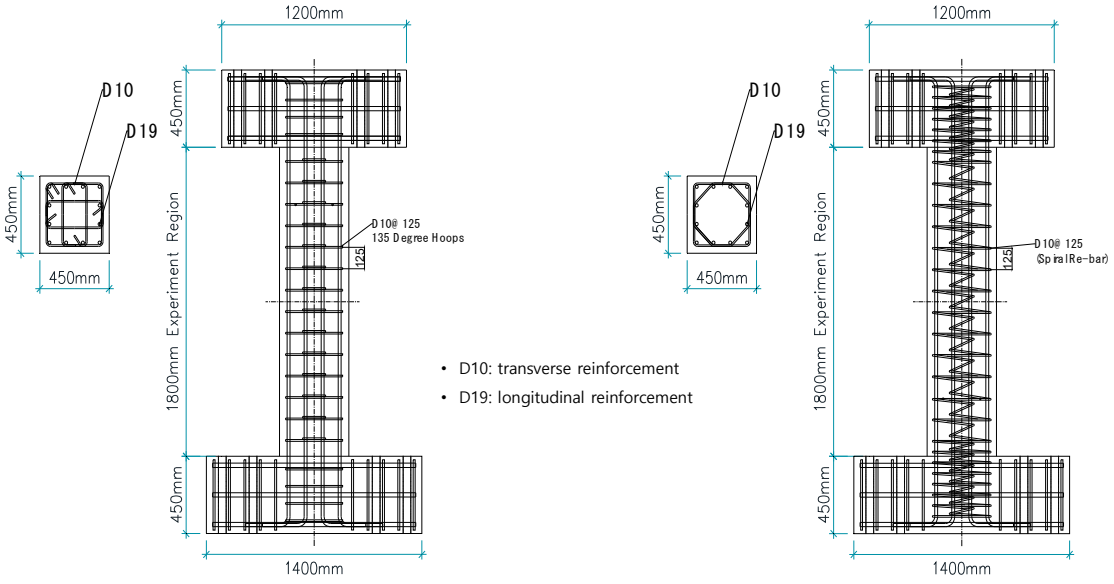

(**a**) (**b**)

Figure 1. Details of specimens (Unit: mm): (**a**) H-F; (**b**) KSS.

All specimens had square cross-sections with width (B) of 450 mm and column depth (D) of 450 mm; the shear span to depth ratio (a/d) was set to 2.0. The effective depth (d) was set to 400 mm in consideration of the concrete cover and crosstie diameter. All specimens had four longitudinal reinforcing bars (D19) with yield strength of 523 MPa on each side to prevent shear failure and induce flexural failure due to yielding of longitudinal reinforcement before other types of failure. Transverse reinforcements (D10) were arranged at a spacing of 125 mm. In Table 3, the reinforcement

ratio ($\rho_{w.H}$) of each specimen was calculated using the following:

$$\rho_{w.H} = \frac{A_{s.H}}{B \cdot s} \quad (1)$$

$$\alpha = \frac{v_{KSS}}{v_H} \quad (2)$$

$$\rho_{w.KSS} = \alpha \cdot \rho_{w.H}. \quad (3)$$

Here, $\rho_{w.H}$ and $\rho_{w.KSS}$ are the transverse reinforcement ratios of specimens with rectangular crossties and specimens with the proposed spiral-type crossties. $A_{s.H}$ is the cross-sectional area of the rectangular crossties, v_H and v_{KSS} are the volume of rectangular crossties and of the proposed spiral-type crossties for transverse reinforcement with spacing s, and α is the ratio of v_{KSS} to v_H.

Since the proposed spiral-type crossties have octagonal sub-ties arranged spirally between rectangular crossties, this study used v_{KSS}/v_H instead of the volume ratio of spiral reinforcement comprised of square or circular steel to calculate the transverse reinforcement ratio $\rho_{w.KSS}$ of KSS specimens, expressing it in terms of the transverse reinforcement ratio of the H-F specimens. Through Equations (1)–(3), KSS specimens were found to have the same ρ_w of 0.0037. These were more advantageous in that the amount of reinforcement was 27% less than that of H-F specimens with the same crosstie spacing s.

2.3. Test Setup and Instrumentation

Using a hydraulic pressure system, the test specimens were subjected to reversed cyclic bending, shear, and axial load in a setup with vertically fixed top and bottom stubs. Lateral force was applied to the loading frame connected to the upper stub. The lateral force actuator, with a loading capacity of 1000 kN, was located so that point of contra flexure is produced at the midspans of the specimens. An axial force corresponding to 15% of the compressive strength of the column was continuously applied using a vertical actuator with a loading capacity of 2000 kN until the end of the test. Figure 2a presents details of the loading and measurement system. Several linear variable displacement transducers (LVDT) were installed to measure the drift angles of specimens. Two LVDTs of 300 mm were installed on the upper and lower stubs of the specimens; average measurements were used to calculate the drift angle. The strain in the transverse and longitudinal reinforcement was measured used strain gauges attached to the reinforcing bar surface. Figure 2b shows the loading protocol used in this testing program. The specimens were loaded monotonically up to the first yield drift angle, δ_y, followed by a series of drift-controlled loading cycles comprising two full cycles with specified drift angles of about $\pm 2\delta_y$, $\pm 3\delta_y$·····. The tests were terminated when the lateral force in the post-peak load-deformation curve dropped to approximately 85% of the peak-recorded load.

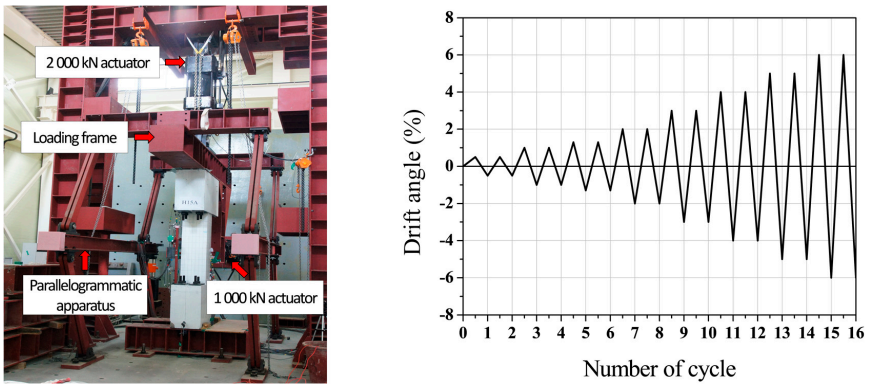

(**a**) (**b**)

Figure 2. View of test setup and loading history: (**a**) Test setup; (**b**) Loading history.

3. Experimental Results and Discussions

3.1. Load Versus Drift Angle Relations

The lateral load vs. drift of the specimens are presented in Figure 3 Quantitative values of measured yield and maximum load, and drift angles, are given in Table 4. It was observed that the longitudinal reinforcement of specimen H-F yielded at a drift angle of −1.24%, and the load reached the maximum value at −441.4 kN at the drift angle of −1.88% in the negative direction. At the drift angle of −4.01%, where the load dropped below 80% of the maximum load, the test was terminated. On the other hand, longitudinal reinforcements of specimens KSS-5, 7, and 12 yielded at drift angles less than −1.04%, earlier than specimen H-F. The average yield load, P_y, of specimens KSS-5, 7, and 12 was about 3.1% lower than that of specimen H-F, while the average maximum load of the specimens was very similar to that of specimen H-F. The effective stiffness of the specimens with KSS at yield load increased as the yield strength of the transverse reinforcement increased. After peak load, the strength of specimen KSS-7 dramatically decreased, to below 80% of the maximum strength, and thus the test was finished at the drift angle of −3.08%. The observed ductility of specimen KSS-7 is lower than that of the other specimens. It was confirmed that specimen KSS-7 experienced bond failure between longitudinal reinforcement and concrete after maximum load. All specimens showed similar behavior in terms of load vs. drift angle. These experimental results verify that the proposed transverse reinforcement effectively suppressed the lateral expansion of concrete, thereby increasing the maximum strength and ductility of the RC columns.

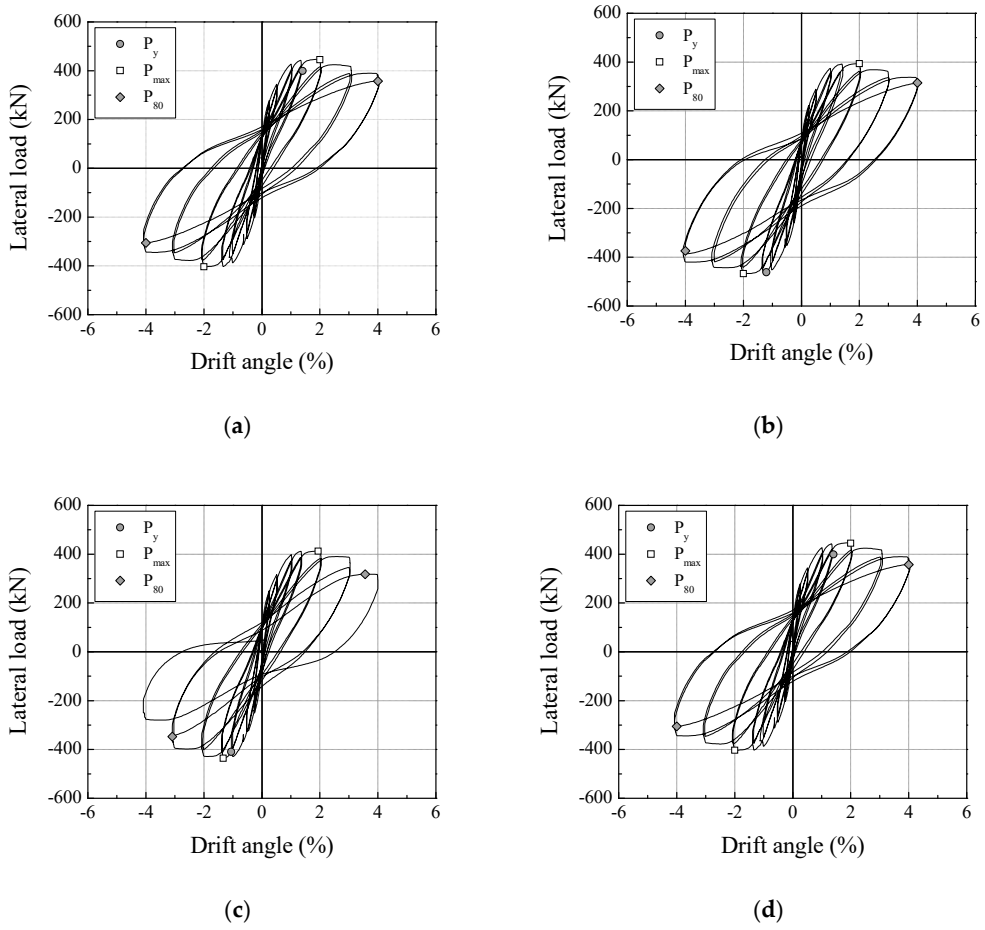

Figure 3. Lateral load versus drift angle relationships: (**a**) H-F; (**b**) KSS-5; (**c**) KSS-7; (**d**) KSS-12.

Table 4. Results of cyclic loading tests.

Specimen	Loading Direction	At Yielding of Reinforcement		At Peak Load		At 0.8 P_{max}		Failure Mode
		P_y (kN)	D_y (%)	P_{max} (kN)	D_{max} (%)	P_u (kN)	D_u (%)	
H-F	Positive	399.3	1.35	407.9	1.87	326.4	4.04	Flexural/Buckling
	Negative	−433.9	−1.24	−441.4	−1.88	−353.1	−4.01	
KSS-5	Positive	380.3	1.49	393.1	1.89	314.5	4.01	Flexural
	Negative	−454.6	−1.16	−467.0	−1.95	−373.6	−4.07	
KSS-7	Positive	409.9	1.64	412.0	1.35	330.1	3.02	Flexural/Bond
	Negative	−409.5	−1.01	−435.8	−1.33	−348.7	−3.08	
KSS-12	Positive	426.8	1.33	439.4	1.78	351.5	4.02	Flexural
	Negative	−418.5	−0.96	−421.6	−1.33	−337.3	−4.10	

Notation-P_y: yield load, P_{max}: maximum load, P_u: ultimate load (0.8 P_{max}), D_y: drift angle at P_y, D_{max}: drift angle at P_{max} and D_u: drift angle at P_u.

3.2. Crack Patterns and Failure Modes

Crack patterns of the specimens at maximum load are shown in Figure 4. In specimens with an axial force ratio of 15%, flexural cracks were first observed at a 0.5% drift angle at both plastic hinge regions. Except for specimen KSS-12, bond cracks appeared along the longitudinal reinforcement, with an increase in the number of flexural cracks when the drift angle Fexceeded 1.0%. In general, bond cracks are observed on RC members when shear span-to-effective depth ratio (a/d) lies within a range of 1.0 to 2.5. In the case of specimen KSS-7, remarkable bond cracks occurred along the longitudinal reinforcement. The bond cracks induced failure of that specimen earlier than for the other specimens after maximum load. Concrete deterioration due to cyclic loading was observed in both plastic hinge regions.

(**a**) (**b**) (**c**) (**d**)

Figure 4. Crack patterns in specimens at failure: (**a**) H-F; (**b**) KSS-5; (**c**) KSS-7; (**d**) KSS-12.

Figure 5 shows the status of reinforcements in the lower plastic hinge region of specimens after the cyclic loading test. It was observed that crossties with 90 and 130-degree standard hooks in specimen H-F became loose due to the lateral expansion of concrete. Furthermore, buckling of the longitudinal reinforcement was observed in the specimen. The buckling of longitudinal reinforcement

degrades the load-carrying capacity of RC structures subjected to seismic loads [28]. Compared with specimens KSS, specimen H-F showed remarkable spalling of concrete cover in the plastic hinge region. In the case of specimens KSS, buckling of longitudinal reinforcement was not observed. This means that the rectangular shear reinforcement and the octagon-shaped sub-ties confined the longitudinal reinforcement and inner concrete until failure. Kani et al. [29] found that when a/d of RC members is smaller than 2.5, the shear resistance of RC members increases significantly. It means that the structural performance of RC members with a/d greater than 2.5 is likely to be determined by the bending resistance. It is well known that using spiral reinforcement can greatly improve the bending capacity of RC columns. Thus, it can be understood that the proposed transverse reinforcement (KSS) is effective at improving the strength and lateral load-carrying capacity of RC columns with a shear span-to-effective depth ratio of more than 2.5.

(**a**) (**b**) (**c**) (**d**)

Figure 5. Observation of reinforcements in plastic hinge region: (**a**) H-F; (**b**) KSS-5; (**c**) KSS-7; (**d**) KSS-12.

3.3. Ductility and Energy Dissipation Capacity

The ductility and energy dissipation capacity of the specimens were experimentally investigated in this study. The effective stiffnesses, the ductility factor (μ), and the energy dissipation capacity for each specimen are given in Table 5. The ductility factor (μ) was taken as the ratio of ultimate story drift, Δ_u, to story drift corresponding to yield load, Δ_y. In this study, a story drift corresponding to 80% of the maximum load was taken as ultimate story drift Δ_u. The energy dissipation, W, was defined as the sum of the area enclosed by the load-story drift curves.

Table 5. Comparison of ductility factor and energy dissipation.

No. (i)	Specimen	$\rho_w f_{wy}$	Effective Stiffness			Ductility Factor		Energy Dissipation	
			$K_{e.y}$	$K_{e.max}$	$K_{e.u}$	μ	μ_i/μ_1	W	W_i/W_1
			(N/mm)	(N/mm)	(N/mm)	(-)	(-)	(J)	(-)
1	H-F	2.75	19,440.0	13,043.7	4891.9	3.23	1.00	148,702.1	1.00
2	KSS-5	2.04	21,772.0	13,304.8	5099.6	3.51	1.08	150,297.2	1.01
3	KSS-7	2.91	22,524.8	18,203.8	6589.7	3.05	0.94	145,008.7	0.98
4	KSS-12	4.90	24,218.8	17,610.7	4570.5	4.27	1.32	164,628.7	1.11

Notation-i: number of specimens, $K_{e.y}$: effective stiffness at yield load, $K_{e.max}$: effective stiffness at maximum load, $K_{e.u}$: effective stiffness at ultimate load.

Although the amount of transverse reinforcement was reduced by about 27%, the effective stiffness of the specimens with KSS at yield load in the negative direction was greater than that of specimen H-F. $K_{e.y}$ increased as the yield strength of transverse reinforcement increased. Specimen KSS-7, moreover, showed the highest effective stiffness at the maximum load and showed the lowest effective stiffness reduction rate among all specimens. In terms of ductility capacity, while specimen KSS-7 showed a

ductility factor similar to that of specimen H-F, specimens KSS-5 and 12 showed a greater ductility factor, which increased in proportion to the yield strength of the reinforcement. The energy dissipation also showed a trend similar to the ductility factor.

Figure 6 uses an index, $\rho_w f_{wf}$, to compare the ductility and energy dissipation capacities of the specimens. Considering that specimen KSS-7 experienced bond failure, it can be understood from Figure 6a that even if the utilized transverse reinforcement ratio, ρ_w, is reduced, the ductility capacity of the RC columns can then be improved by increasing the yield strength of the reinforcement, f_{wf}. Figure 6b presents the ratio of the energy dissipated in specimens with KSS to that dissipated in specimen H-F at each drift angle. As a result of the cyclic loading test, specimen KSS-5, due to its lower effective stiffnesses of up to 3.0% of the drift angle, showed energy dissipations lower than those of specimen H-F; however, both specimens showed similar energy dissipation capacities at the end of the test. Specimen KSS-12 showed the best performance in terms of the ductility and energy dissipation.

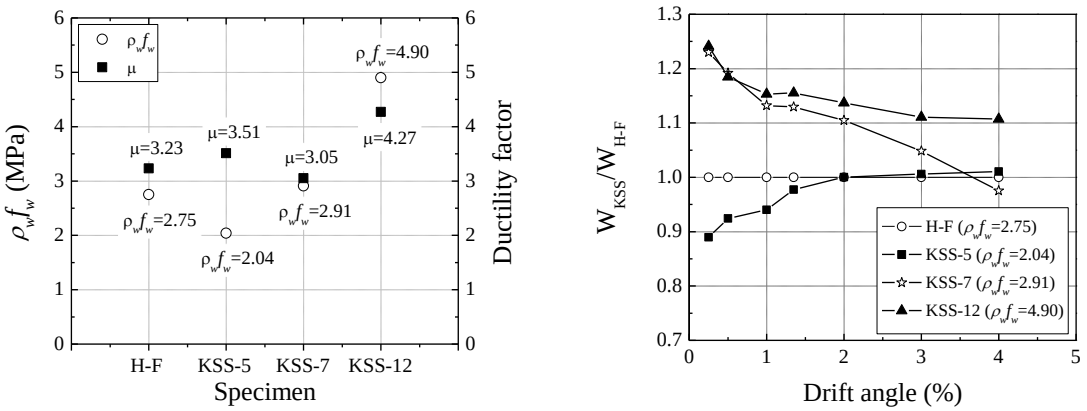

Figure 6. Comparison of ductility factor and energy dissipation: (**a**) Ductility factor; (**b**) Energy dissipation.

It was found that the seismic performance of RC columns with the same cross-sectional property can be enhanced by increasing the yield strength of transverse reinforcement. Furthermore, it is possible to reduce the amount of reinforcing steel used for the construction of reinforced concrete structures if the inner concrete and the longitudinal reinforcement are confined by transverse reinforcement with an appropriate shape.

4. Constructability of Proposed Transverse Reinforcement

This study performed mockup tests to evaluate the constructability of RC columns in relation to the shape of the transverse reinforcement. The arrangement of transverse reinforcement was done by skilled workers; constructability between H-F and KSS specimens was compared based on the assembly time of the transverse reinforcement. The specimens were fabricated considering the cross-sections of columns in actual RC structures. Table 6 presents information on specimen cross-sections and arrangement details, and assembly times of transverse reinforcement measured during the mockup tests. The average assembly time of transverse reinforcement was 56 min 12 s for H-F specimens, and 21 min 12 s for KSS specimens. The assembly time for transverse reinforcement of KSS specimens was 60% faster than that of H-F specimens. This is because KSS specimens pull down transverse reinforcement from the top of longitudinal reinforcement in a spring-like manner to fit the given spacing, whereas H-F specimens introduce 90 and 130-degree standard hooks between transverse reinforcement after completing the arrangement of transverse reinforcement. The evaluation of structural performance and constructability showed that the proposed transverse reinforcement will have advantages over conventional rectangular reinforcement in terms of reduced amount of reinforcement in fabricating column members and improved constructability.

Table 6. Comparison of constructability between H-F and KSS.

Specimens	BxD (mm)	H (mm)	s (mm)	1st	2nd	3rd	Average
H-F	500 × 500	3500	135	43′40″	56′50″	68′06″	56′12″
KSS				20′32″	21′35″	21′30″	21′12″
KSS/H-F				47.0%	38.0%	31.6%	37.7%

5. Conclusions

In this study, an experiment was conducted to evaluate the flexural performance of RC columns confined with a newly developed spiral type transverse reinforcement (KSS). Experimental results were compared with an RC column confined with a conventional hoop reinforcement. The experimental results showed that KSS transverse reinforcement, due to its superior confinement effect for concrete and longitudinal reinforcement, increases the effective stiffness of columns at yield and maximum strength. Moreover, the results showed that the ductility and energy dissipation capacities of RC columns with KSS were improved compared with those of an RC column with conventional hoops, even though the amount of reinforcement used decreased by about 27%. Finally, it was found that KSS is effective at reducing the amounts of steel and time required to arrange transverse reinforcement.

Author Contributions: Investigation, D.-H.K.; Supervision, K.-H.K.; Writing—original draft, H.-G.K.; Writing—review & editing, C.-Y.J. All authors have read and agreed to the published version of the manuscript.

Funding: This work was supported by the Priority Research Centers Program through the National Research Foundation of Korea (NRF) founded by the Ministry of Education (2019R1A6A1A03032988); This research was supported by Basic Science Research Program through the National Research Foundation of Korea (NRF) founded by the Ministry of Education (2018R1A2B3001656); This research was supported by the Basic Science Research Program through the National Research Foundation of Korea (NRF) founded by the Ministry of Education (2019R1I1A3A01058156); This work was also supported by a research grant of the Kongju National University in 2020 (2020-0203-01).

Conflicts of Interest: The authors declare no conflict of interest.

References

1. Marinez, S.; Nilson, A.H.; Slate, F.O. Spirally Reinforced High-Strength Concrete Columns. *ACI Struct. J.* **1984**, *8181*, 431–442.
2. Moehle, J.; Cavanagh, T. Confinement Effectiveness of Crossties in RC. *J. Struct. Div.* **1985**, *111*, 2105–2120. [CrossRef]
3. Mander, J.B.; Priestley, M.J.N.; Park, R. Observed Stress-Strain Behavior of Confined Concrete. *J. Struct. Eng.* **1988**, *114*, 1827–1849. [CrossRef]
4. Yong, Y.K.; Nour, M.G.; Nawy, E.G. Behavior of Laterally Confined High-Strength Concrete Under Axial Loads. *J. Struct. Eng.* **1989**, *114*, 332–351. [CrossRef]
5. Muguruma, H.; Watanabe, F. Ductility Improvement of High-Strength Concrete Columns with Lateral Confinement. *ACI Spec. Publ.* **1990**, *121*, 47–60.
6. Muguruma, H.; Watanabe, F.; Tanaka, H. Ductile Behaviour of High-Strength Columns Confined by High-Strength Transverse Reinforcement. *ACI Spec. Publ.* **1991**, *128*, 877–891.
7. Razvi, S.R. Strength and Ductility of Confined Concrete. *J. Struct. Eng.* **1992**, *118*, 1590–1607.
8. Sheikh, S.A.; Toklucu, M.T. Reinforced Concrete Columns Confined by Circular Spirals and Hoops. *ACI Struct. J.* **1993**, *90*, 542–553.
9. Cusson, D.; Paultre, P. High-Strength Concrete Columns Confined by Rectangular Ties. *J. Struct. Eng.* **1994**, *120*, 783–804. [CrossRef]
10. Razvi, S.R.; Saatcioglu, M. Circular High-Strength Concrete Columns under Concentric Compression. *ACI Struct. J.* **1999**, *96*, 817–825.
11. Mander, J.B.; Priestley, M.J.N.; Park, R. Theoretical Stress-Strain Model for Confined Concrete. *J. Struct. Eng.* **1988**, *114*, 1804–1826. [CrossRef]

12. Cusson, D.; Paultre, P. Stress-Strain Model for Confined High-Strength Concrete. *J. Struct. Eng.* **1995**, *121*, 468–477. [CrossRef]
13. El-Dash, K.M.; Ahmad, S.H. A model for stress-strain relationship of spirally con_ned normal and high-strength concrete columns. *Mag. Concr. Res.* **1995**, *47*, 177–184. [CrossRef]
14. Hoshikuma, J.; Kawashima, K.; Nagaya, K. A Stress-Strain Model for Reinforced Concrete Columns Confined by Lateral Reinforcement. *Doboku Gakkai Ronbunshu* **1995**, *520*, 1–11. (In Japanese) [CrossRef]
15. Razvi, S.; Saatcioglu, M. Confinement Model for High-Strength Concrete. *J. Struct. Eng.* **1999**, *125*, 281–289. [CrossRef]
16. Li, B.; Park, R.; Tanaka, H. Stress-Strain Behavior of High-Strength Concrete Confined by Ultra-High- and Normal-Strength Transverse Reinforcement. *ACI Struct. J.* **2001**, *98*, 395–406.
17. Mendis, P.; Pendyala, R.; Setunge, S. Stress-Strain Model to Predict the Full-range Moment Curvature Behavior of High-Strength Concrete Sections. *Mag. Concr. Res.* **2000**, *52*, 227–234. [CrossRef]
18. Kim, Y.S.; Kim, S.W.; Lee, J.Y.; Lee, J.M.; Kim, H.G.; Kim, K.H. Prediction of Stress-Strain Behavior of Spirally Confined Cocrete Considering Lateral Expasion. *Constr. Build. Mater.* **2016**, *102*, 743–761. [CrossRef]
19. Tanaka, H.; Park, R. Strnegth and Ductility of Reinforced Concrete Columns with Interlocking Spirals. In Proceedings of the Tenth World Conference on Earthquake Engineering, Balkema, Rotterdam, 19–24 July 1992; pp. 4371–4376.
20. Tanaka, H.; Park, R. Seismic Design and Behavior of Reinforced Concrete Columns with Interlocking Spirals. *ACI Struct. J.* **1993**, *90*, 192–203.
21. Khaloo, A.R.; El-Dash, K.M.; Ahmad, S.H. Modeling for Lightweight Concrete Columns Confined by Either Single Hoops or Interlocking Double Spirals. *ACI Struct. J.* **1999**, *96*, 883–891.
22. Kim, J.K.; Park, C.K. The Behavior of Concrete Columns with Interlocking Spirals. *Eng. Struct.* **1999**, *21*, 945–953. [CrossRef]
23. Tan, T.H.; Yip, W.K. Behavior of Axially Loaded Concrete Columns Confined by Elliptical Hoops. *ACI Struct. J.* **1999**, *96*, 967–971.
24. Benzaid, R.; Mesbah, H.; Chikh, N.E. FRP-confined Concrete Cylinders: Axial Compression Experiments and Strength Model. *J. Reinf. Plast. Comp.* **2010**, *29*, 2469–2488. [CrossRef]
25. Yin, S.Y.L.; Wu, T.L.; Liu, T.C.; Sheikh, S.A.; Wang, R. Interlocking Spiral Confinement for Rectangular Columns. *Concr. Int.* **2011**, *33*, 38–45.
26. Chen, Y.; Feng, J.; Yin, S. Compressive Behavior of Reinforced Concrete Columns Confined by Multi-Spiral Hoops. *Comput. Concr.* **2012**, *9*, 341–355. [CrossRef]
27. Guo, Y.C.; Xiao, S.H.; Luo, J.W.; Ye, Y.Y.; Zeng, J.J. Confined Concrete in Fiber-Reinforced Polymer Partially Wrapped Square Columns: Axail Compressive Behavior and Strain Distributions by a Particla Image Velocimetry Sensing Technique. *MDPI Sens.* **2018**, *18*, 4118. [CrossRef]
28. Bechtoula, H.; Kono, S.; Watanabe, F. Experimental and Analytical Investigations of Seismic Performance of Cantilever Reinforced Concrete Columns Under Varying Transverse and Axial Loads. *J. Asian Archit. Build. Eng.* **2005**, *4*, 467–474. [CrossRef]
29. Kani, M.W.; Huggins, M.W.; Wittkopp, R.R. *Kani on Shear in Reinforced Concrete*; Department of Civil Engineering, University of Toronto: Toronto, ON, Canada, 1979.